Journal of *Marine Science and Engineering*

MDPI

Article

Mitigation of Vortex-Induced Vibration of Cylinders Using Cactus-Shaped Cross Sections in Subcritical Flow

Jialu Wang [1], Fabo Chen [1], Chen Shi [1,*] and Jiuzheng Yu [2]

[1] College of Petroleum Engineering, China University of Petroleum (East China), Qingdao 266580, China; upc_wangjialu@hotmail.com (J.W.); chenfabo1026@hotmail.com (F.C.)
[2] Oil&Gas Technology Research Institute of Changqing Oilfield Company, Xi'an 710018, China; yujzh_cq@petrochina.com.cn
* Correspondence: shichen2004@hotmail.com; Tel.: +86-156-2102-0406

Abstract: Flexible cylinders, such as marine risers, often experience sustained vortex-induced vibrations (VIVs). Installing helical strakes on a riser is the most widely used technique to mitigate VIVs. This study was inspired by the giant Saguaro Cacti which can withstand strong wind with a shallow root system. In this study, numerical simulations of flow past a stationary cylinder of a cactus-shaped cross-section in a two-dimensional flow field at a subcritical Reynolds number of 3900 were performed. Results show that cylinders of a cactus-shaped cross-section have a lower lift coefficient without increasing drag compared to those of a circular cylinder. VIV experiments on a single flexible pipe as well as on a set of two tandem-arranged flexible pipes were conducted at different reduced velocities to investigate the effects of the streamwise spacing and wake of the cactus-like body shape on VIV mitigation. Experimental results show that the cactus-like body shape can mitigate VIV responses of the cylinder at upstream position with no cost of increased drag; however, similar to helical strakes, the efficiency of VIV mitigation for the cylinder at downstream position is reduced. Although the cactus-like body shapes tested in this study were not optimized for oscillation suppression, still this study suggests that modification of the cross-sectional shape to a well-designed cactus-like shape has potentials to be used as an alternative technology to mitigate VIV of marine risers.

Keywords: vortex-induced vibration; cactus-shaped cross section; marine riser; tandem arrangement

Citation: Wang, J.; Chen, F.; Shi, C.; Yu, J. Mitigation of Vortex-Induced Vibration of Cylinders Using Cactus-Shaped Cross Sections in Subcritical Flow. *J. Mar. Sci. Eng.* **2021**, *9*, 292. https://doi.org/10.3390/jmse9030292

Academic Editors: Alessandro Antonini and Abbas Khayyer

Received: 31 January 2021
Accepted: 4 March 2021
Published: 7 March 2021

1. Introduction

With continuous increases in energy consumptions and the depletion of onshore hydrocarbon resources, explorations and production of oil and gas have been moving to deep waters. Offshore structures often consist of components of a bluff cross section. When water flows past such a bluff body, vortices are formed and shed alternatively at its lee side, which causes pressures around the circumference of the bluff body to vary with time. If the structural component is slender or free to vibrate, it can be excited by the alternating pressures to oscillate both in the direction of the current (termed "in-line"(IL) direction) and in the direction transverse to the direction of the current (termed "cross-flow"(CF) direction). The so-called vortex-induced vibrations (VIVs) are often observed on slender marine structures, such as risers, suspended sections of pipelines, pull tubes, slender truss elements, etc. Sustained VIV of risers may shorten the fatigue life of risers, cause clash and structural failure of risers and, thus, may result in a great economic loss and environmental pollution.

Helical strakes and fairings are often used to suppress VIV. Installing helical strakes on a bare riser can effectively suppress VIV, while at the cost of increased drag force which results in large rotational angles and bending moments at riser hang-off location and wellhead. Excessive rotational angles at those locations may cause shutdown of the drilling or production and even structural failure. The benefit of using fairings is that its drag is

not as large as that of the helical strakes. However, fairings are cumbersome in terms of storage, installation, and maintenance. Especially, fairings cannot be installed on buoyancy modules of risers, which limits its application. It is desirable to invent a technology or device which is effective on suppressing VIV, easy to install, free of maintenance, and have a relatively low drag coefficient. This study was inspired by the giant Saguaro Cacti (as shown in Figure 1) which grow in desert areas. The giant Saguaro Cactus can grow up to 50 feet. It has a shallow root system but can withstand strong winds, which means that the giant Saguaro Cactus has superior aerodynamic characteristics. Several studies have been carried out to investigate the aerodynamic loads of cactus-shaped cylinders through experimental or computational fluid dynamics (CFD) methods [1–4]. AMOG consulting developed an innovative buoyancy module which has a cactus-like cross-sectional body shape called Longitudinally Grooved Suppression (LGS). Water tank experiments have been conducted on the LGS buoyancy modules in large Reynolds Number flow field, and the results showed that the cylinder of a cactus-shaped cross section can reduce VIV responses and drag forces on it simultaneously [5].

Figure 1. The Giant Saguaro Cactus and its cross section.

In deepwater deployments several risers are often placed together as an array of risers. Hydrodynamic responses of a riser in an array are different and much more complicated than those of an isolated riser. As the simplest case of a riser array, two tandem-arranged cylinders were studied through numerical simulations, and the flow patterns, hydrodynamic loads, and the effects of the spacing between the two cylinders were investigated [6–8]. The comprehensive studies on a pair of two cylinders, either of a tandem- or staggered-arrangement, were conducted through water tunnel experiments by Assi and their group [9,10]. It was concluded that the vibration of the downstream cylinder was excited by the unsteady vortex-structural interaction between the cylinder and the vortices coming from the upstream cylinder and, thus, is termed wake-induced vibration (WIV). The excitation force on the downstream cylinder consists of two parts: one is associated with the "wake-stiffness", the other is associated with the impulse vortex-force; magnitudes of both terms depend on the relative position of the downstream cylinder in the wake of the upstream cylinder. Indeed, WIV of the downstream cylinder is a "wake-excited and wake-sustained" flow-induced vibration. Another study conducted by Huang and Sworn [11] on the two fixed cylinders fitted with helical strakes showed that the helical strakes can reduce VIV responses; however, the efficiency of WIV suppression on the downstream cylinder is negatively affected by the wake shed from the upstream cylinder.

In this study, a steady current flowing past a stationary cylinder was simulated in a two-dimensional flow field at a subcritical Reynolds number of 3900 by using the commercial software ANSYS FLUENT. Two types of cross sections, circular and cactus-shaped cross sections, were studied. The effects of the number and the height of ridges of

cactus-shaped cross sections on the hydrodynamic coefficients were investigated. When VIV happens, vortex-shedding not only occurs in the plane perpendicular to the axis of the cylinder, but also travels along the axis of the cylinder and synchronizes spatially. The inherent three-dimensional features of VIV cannot be captured by two-dimensional simulations. Moreover, VIV is featured by nonlinear fluid-structure interactions. The movement of the oscillatory body influences the vortex formation and shedding which, in turn, affect the dynamic responses of the body. When the oscillatory amplitude of the CF movement reaches to 0.2 or 0.3 times of the body's diameter, the IL responses will be significantly magnified by the movement in the CF direction [12]. Meanwhile, the IL movement affects vortex mode and the CF responses. A body free to oscillate in both the CF and the IL directions has a larger CF amplitude than that of only CF movement allowed [13–16]. Strictly speaking, the dynamic responses of an oscillatory cylinder experiencing VIV cannot be thoroughly investigated using numerical simulations on a stationary cylinder. However, the purpose of using numerical simulations is to screen suitable candidates for experimental studies. Next, a flexible pipe of a cactus-shaped cross section was tested over a range of reduced velocity from 2 to 14 in a water tank facility. Comparisons with the cylinder of a circular cross section show that the cylinder of a cactus-shaped cross-sections has lower VIV responses. Experiments on a set of two tandem-arranged cylinders were also conducted, and the results show that the cactus-shaped cross-sectional body shape can suppress VIV responses of the upstream cylinder; while, compared with the upstream cylinder, the suppression efficiency is reduced for the downstream cylinder placed in the wake of the upstream cylinder. Simulation and experimental results indicates that the cactus-shaped cross-sectional body shape, if well designed, have a potential to be used as an alternative technology to suppress VIV of marine risers. It is worth mentioning that the Reynolds number affects the flow pattern and hydrodynamic forces on a cylinder. Numerical simulations and experimental studies show that the oscillatory amplitude of a cylinder experiencing VIV increases with increasing Reynolds number [17,18]. Some recent experimental studies are conducted either in air or in water to investigate the VIV responses of a cylinder at high Reynolds numbers [19,20]. The temporary conclusions drawn from the present study at subcritical flow regime need to be further investigated before being applied on marine structures exposed to real ocean current with a Reynolds number in the upper subcritical and the transitional regimes (about 10^5 to 10^6).

2. Simulation Model Setup

Commercial software ANSYS FLUENT was used to simulate a stationary cylinder in a two-dimensional flow field of the subcritical Reynolds number of 3900. Two types of cylinders were studied: (a) a cylinder of a circular cross section with an outer diameter of $D = 0.1$ m as a reference case and, (b) cylinders of a cactus-shaped cross section with n ridges. As shown in Figure 2, the inscribed circle (represented by a dotted line) of the cactus-shaped cross section has a diameter of D, which is the same as the diameter of the circular cross section. The height of ridges, h, which is the radial distance from the highest point of ridges to the lowest point of grooves. The geometry of the ridge element was determined using curve-fitting of each "peak" and "dip" by cubic splines, thus, the outermost diameter of the cross section is $D + 2h$. In this study, the number of ridges varies as $n = 8, 12, 16, 20, 24$ and the height of ridge varies as $h = (0.02, 0.04, 0.06, 0.08)D$. For example, the cylinder of a cactus-shaped cross section with 8 ridges and the height of ridges $h = 0.04D$ is labeled as R8-0.04; as a result, twenty cactus-shaped cylinders of different number and height of ridges were simulated and compared with the reference case, i.e. the cylinder of a circular cross section labeled as R0.

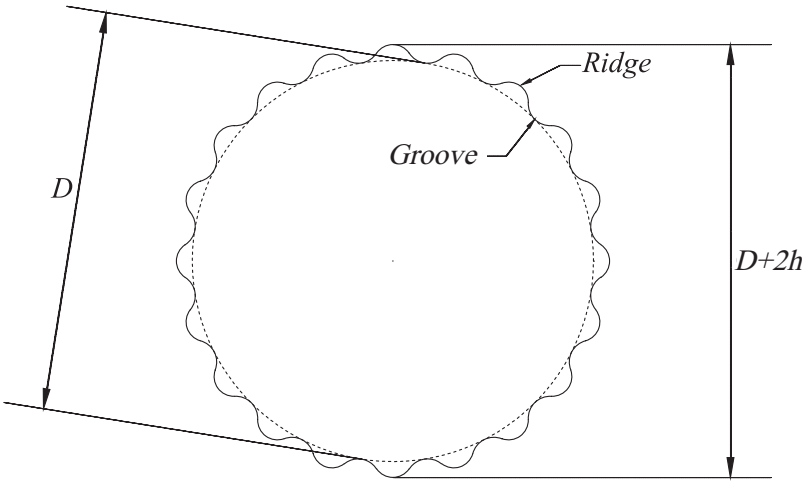

Figure 2. The cactus-shaped cross section with 20 ridges.

As shown in Figure 3, a two-dimensional uniform flow field was simulated with a dimension of 16D by 28D, where D is the outer diameter of the circular cross section. Water flows from left to right, which means that the left boundary is the velocity inlet and the right boundary is the pressure outlet. Water velocity at the inlet boundary was set to be 0.0392 m/s which corresponds to the Reynolds number of 3900 for the cylinder of a circular cross section. For all simulation runs the water velocity remains unchanged as 0.0392 m/s resulting in the Reynolds number slightly larger than 3900 for cylinders of a cactus-shaped cross section due to their larger characteristic length; however, effects of a small difference of the Reynolds number on simulation results were assumed negligible. The upper and lower boundaries of the numerical domain of the flow field were set as a slip condition. In the flow field, a stationary cylinder, of either a circular cross section or a cactus-shaped cross section, was positioned 8D from the inlet boundary and in the middle between the lower and upper boundaries of the numerical domain. The turbulence model SST-Kω with Low-Re correction was selected for simulations.

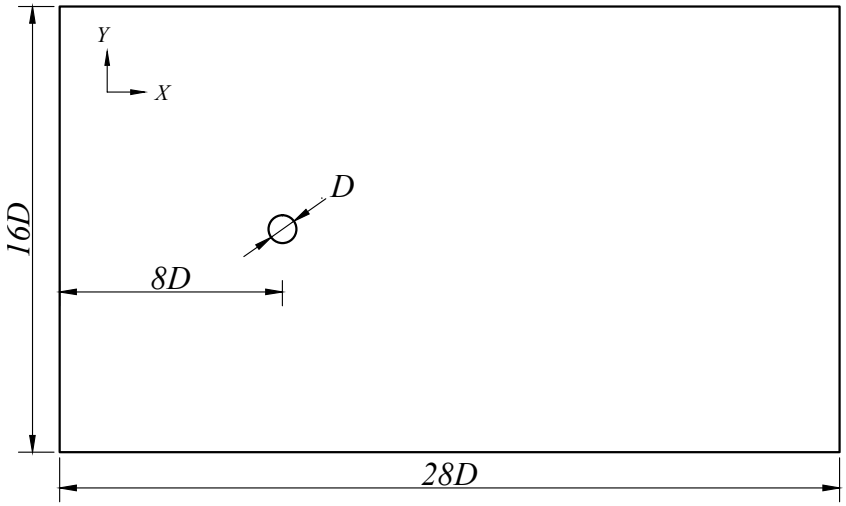

Figure 3. Simulated two-dimensional flow field.

The entire flow field was divided into several sub-regions as shown in Figure 4. The sub-region which surrounds the cylinder was most densely meshed using unstructured grids to suit the complex boundary of the cylinder, especially the one of the cactus-shaped cross section. The size of the first layer grids near the cylinder was strictly controlled to make sure the value of y^+ was less than 1.0. The mesh of the "wake" sub-region was a little bit coarse; and the meshes of the rest regions were even coarser compared with the

two previous sub-regions. Except for the sub-region surrounding the cylinder, the wake and all the other sub-regions were meshed using structured grids; and the mesh quality in terms of the minimum orthogonal quality, maximum ortho-skew, and maximum aspect ratio were all checked to ensure the accuracy, speed, and convergence of simulations. Note that procedures of meshing were same for the circular and cactus-shaped cylinders.

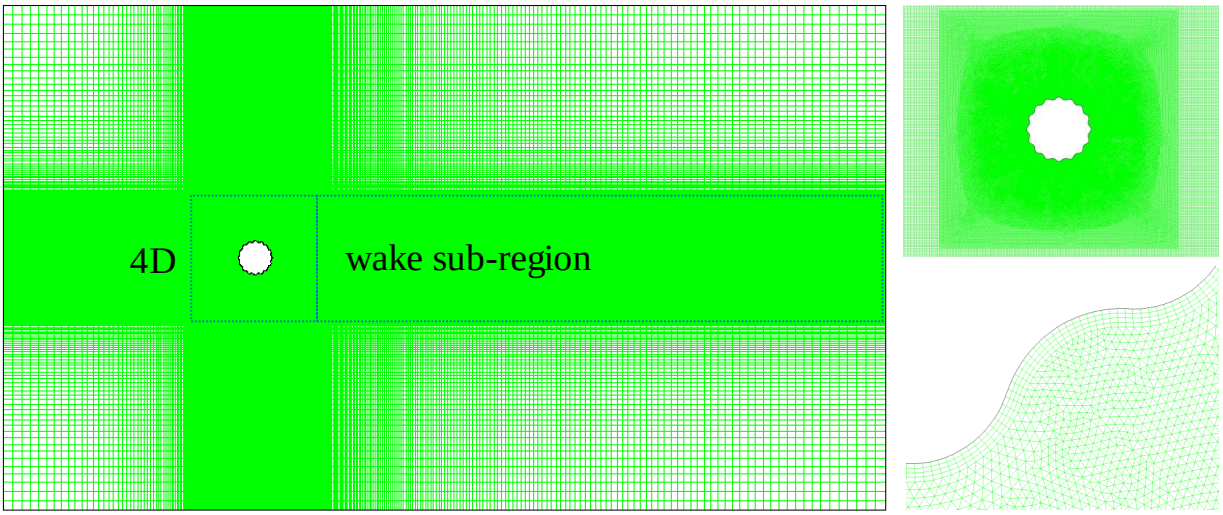

Figure 4. Mesh of the flow field for simulation runs of a single cylinder of a cactus-shaped cross section.

A sensitivity study on the number of grid points was conducted for simulations on a circular cylinder. The total number of grid points of the entire flow field increases from about 50,000 to 200,000. For each simulation run, the root-mean-square (RMS) value of the lift force, F_L, and the mean value of the drag force, F_D, exerted on the cylinder were obtained after the simulation became stable and, then, the lift coefficient, C_L, and drag coefficient, C_D, were calculated using equations $C_L = F_L/(\frac{1}{2}\rho u^2 S)$ and $C_D = F_D/(\frac{1}{2}\rho u^2 S)$, respectively; where, ρ is the fluid density, u is the mean fluid velocity, and S is the reference length. The Strouhal number, St, was also calculated by using the equation $St = fS/u$, where, f is the frequency of vortex shedding. In this study the reference length, S, of both the circular and cactus-shaped cylinders, was set to the same value of D which is the outer diameter of the circular cross section, regardless of the outermost diameter of the cactus-shaped cross section is $D + 2h$. By this way, the lift coefficient, C_L, drag coefficient, C_D, and Strouhal number, St, of the cactus-shaped cylinders can be compared directly with those parameters of the circular cylinder. Note that the "real" values of C_L and C_D of the cactus-shaped cylinders should be smaller than values presented in this study if the "correct" reference length, $D + 2h$, was used for calculations. Lift and drag coefficients and Strouhal number of a single circular cylinder obtained from simulation runs using different number of grid points were presented in Table 1. Assuming the number of grid points of 200,000 as a reference case, the differences of C_L , C_D, and St between other simulation runs and the reference case were also calculated. If assume 1.0% of difference as the threshold value, the simulation using 160,000 grid points were thought to be accurate enough. In this study, the total number of grid points of the entire flow field was set to be about 160,000 for all simulations, regardless of the cross-sectional shape of the cylinders (either circular or cactus-shaped).

Table 1. Sensitivity study on the number of grids for simulations on a single circular cylinder at the Reynolds number of $Re = 3900$.

Number of Grid	C_D	C_L	S_t
40,000	1.65	1.17	0.25
80,000	1.21	0.64	0.23
120,000	1.16	0.53	0.20
160,000	1.05	0.30	0.21
200,000	1.04	0.29	0.21

In order to verify the model, a simulation run on a circular cylinder at a subcritical Reynolds number of $Re = 3900$ was carried out and compared with the results obtained by other researches. As presented in Table 2, the hydrodynamic coefficients, including the lift, C_L, drag, C_D, and Strouhal number, St, simulated using the present model match the results of other studies [21,22].

Table 2. Hydrodynamic coefficients of a single circular cylinder simulated for a subcritical Reynolds number ($Re = 3900$) flow field: Comparison between the present model and the results of other studies [21,22].

Hydrodynamic Coefficients	Fröhlich et al.	F.S. Pereira et al.	Present Model
C_L	0.30	0.28	0.30
C_D	1.17	1.04	1.05
St	0.21	0.21	0.21

3. Simulation Results

Vortex-shedding from a stationary cylinder of either a circular cross section or a cactus-shaped cross section in a two-dimensional flow field of the Reynolds number of $Re = 3900$ was simulated. By varying the number of ridges, n, between 8 and 24, and the height of ridges, h, between $0.02D$ and $0.08D$, in which D is the outer diameter of the circular cross section, twenty different cactus-shaped cross sections were evaluated, and their effects on the lift coefficient, C_L, drag coefficient, C_D, and Strouhal number, St, were illustrated in Figure 5.

As shown in Figure 5a, the lift coefficient of the circular cylinder, represented by a solid line, is 0.30. For cactus-shaped cylinders of 8 and 12 ridges, the lift coefficients increase with the height of ridge and decrease with the number of ridge; for cactus-shaped cylinders of 16, 20, and 24 ridges, the lift coefficients decrease to a value around 0.2 which is lower than the value of the circular cross-section and remain unaffected by the number and height of ridge of the cactus shapes. Drag coefficients of the cylinders were plotted in Figure 5b, in which most of the drag coefficients of cactus-shaped cylinders are larger than that of the circular cylinder which is represented by the solid line at a value of 1.05. Generally, drag coefficients slightly decrease with the number of ridge and increase with the height of ridge of the cactus shapes. Recall that in this study the reference lengths used in the calculation of C_L and C_D for both the circular and cactus cylinders, were set to the same value of D which is the outer diameter of the circular cross-section, regardless of the outermost diameter of the cactus-shaped cross-section is $D + 2h$. If the "correct" values of reference length, $D + 2h$, were used, the C_L and C_D calculated on the cactus-shaped cylinders shall be smaller than the values plotted in Figure 5. Strouhal number, St, of the cactus-shaped cylinders were also compared with that of the circular cylinder. As plotted in Figure 5c, cactus-shaped cylinders have smaller Strouhal numbers than that of the circular cylinder, which indicates that cactus cross-sectional body shape can interfere with vortex generation and reduce the frequency of vortex shedding. Results showed that the cactus-like cross-sectional body shape may be used to suppress VIV response of marine structures.

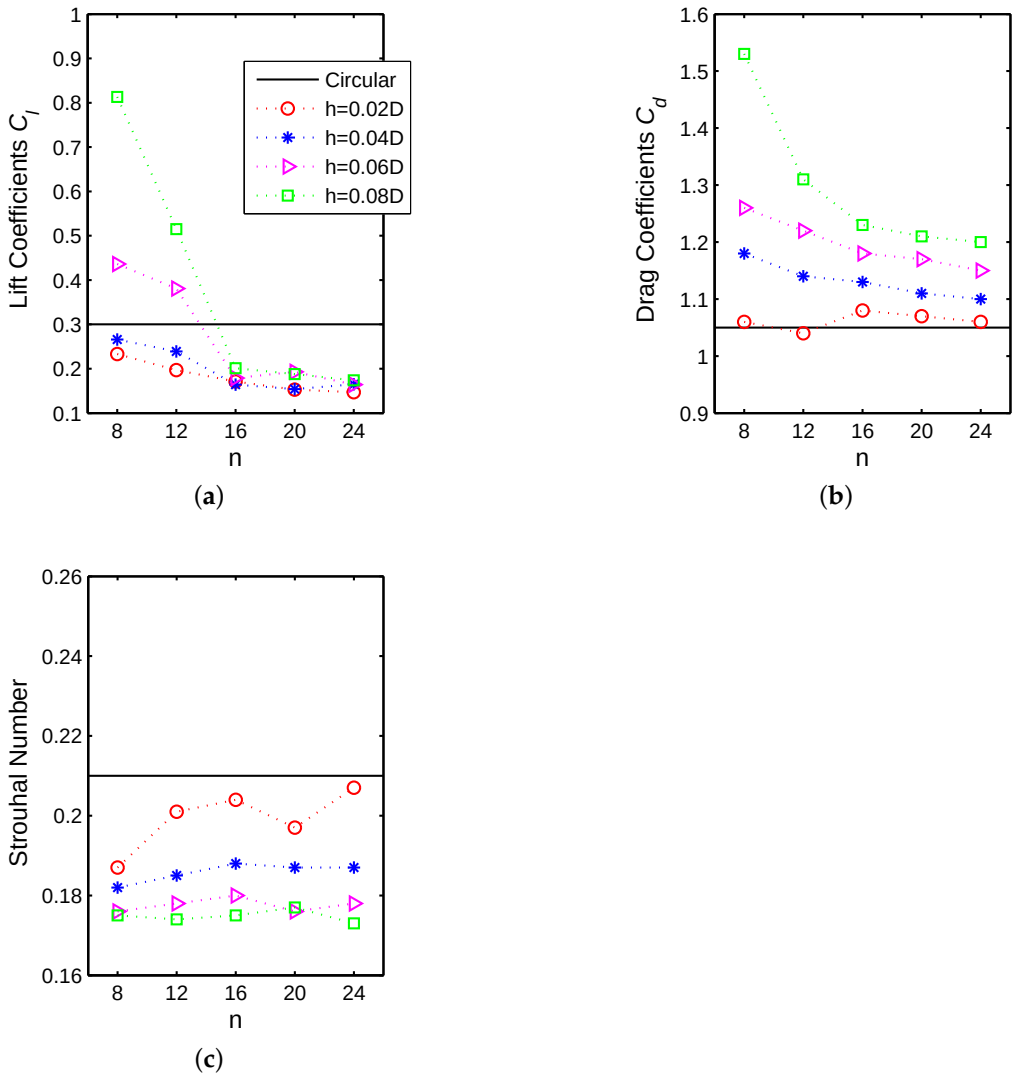

Figure 5. Hydrodynamic coefficients of a stationary cactus-shaped cylinder simulated in a two-dimensional flow field: (**a**) lift coefficients, C_l, (**b**) drag coefficients, C_d, and (**c**) Strouhal number, S_t.

The cactus-shaped cylinder, *R*8-0.04, having 8 ridges with the height of ridges equals to $h = 0.04D$, was used as an example to illustrate the mechanism of the VIV suppression of the cactus-like body shape. As shown in Figure 6, snapshots of contours of the current vorticity magnitudes around a single stationary cylinder were taken at the instant of the lift coefficient reaches the maximum value, where the upper figure is for the cactus-shaped cylinder, *R*8-0.04, and the lower figure is for the circular cylinder, *R*0. Compared to the circular cylinder, vortices shed from the cactus-shaped cylinder are more sparsely spaced and each vortex contains fewer contour lines, which means that the shedding frequencies and energies of the vortices are smaller. Figure 7 illustrates that the flow pattern near the surface of the cactus-shaped cylinder was significantly changed by the presence of ridges. A recirculation filled between neighboring ridges impedes the formation of regular vortices. It also repels the vortices off the cylinder's surface which reduces the shear stress and pressure on the surface of the cylinder, which may explain the VIV mitigation effect of the cactus-like body shape [4].

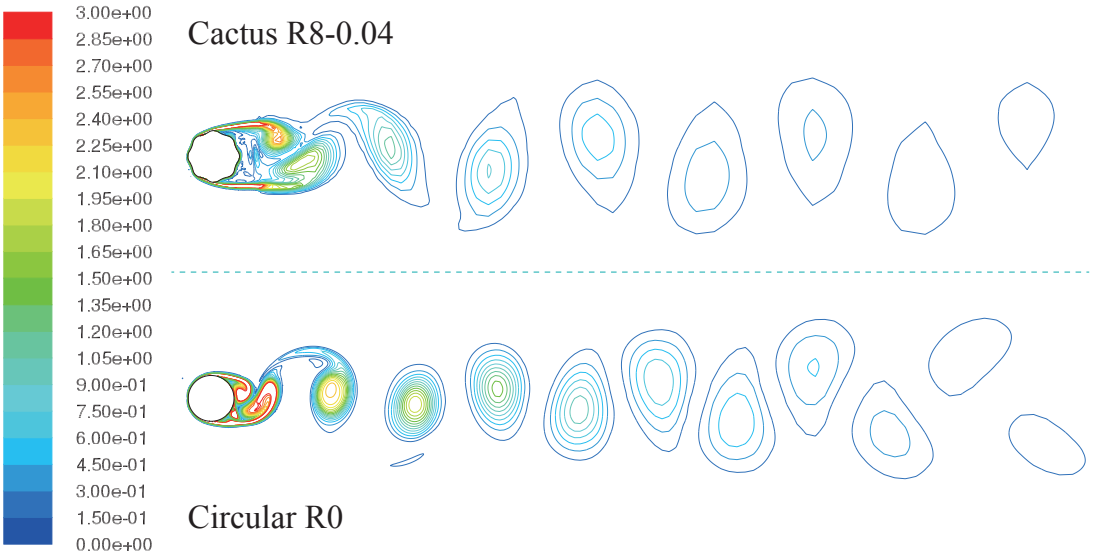

Figure 6. Contours of the current vorticity magnitudes around a single stationary cylinder at the Reynolds number of $Re = 3900$: a circular cross-section, *R*0 (**lower**), and a cactus-shaped cross section, *R*8-0.04 (**upper**).

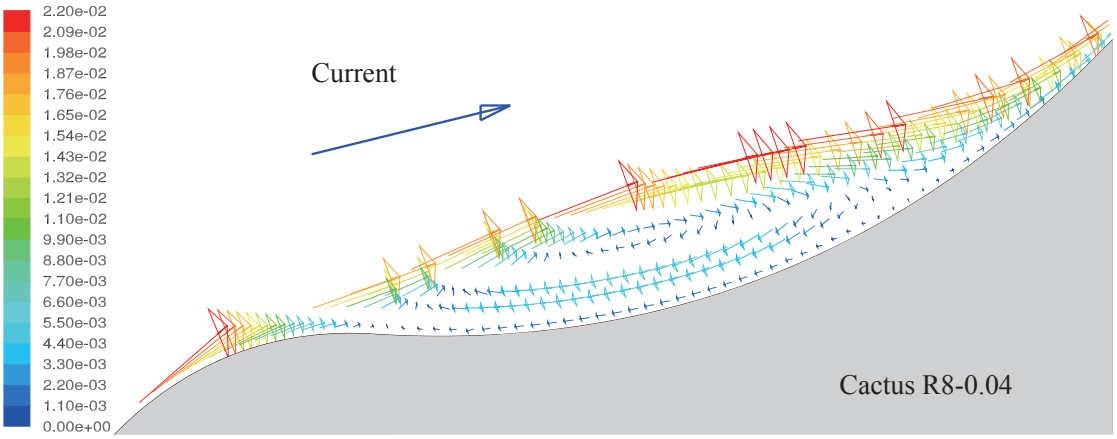

Figure 7. Velocity vectors of current flow near the ridges of cactus-shaped cylinder, *R*8-0.04.

Note that if a cylinder is free to oscillate, oscillations in the cross-flow direction generally will amplify the drag force [23] and the VIV responses are expected to be different compared to a stationary cylinder. In addition, when VIV happens, vortex-shedding not only occurs in the plane perpendicular to the axis of the cylinder, but also travels along the axis of the cylinder and synchronizes spatially. The inherent three-dimensional features of VIV cannot be captured by two-dimensional simulations. Thus, in this study, water tunnel experiments were conducted to comparing VIV responses of the same flexible pipe with different cross-sectional shapes.

4. Experimental Setup

Experimental tests were conducted at the water tunnel facility located in the Ocean Engineering Laboratory of China University of Petroleum (East China). The water tunnel has a rectangular cross section with a width of 1.0 m and a height of 1.5 m (see Figure 8), and a uniform flow with the maximum current speed of 0.4 m/s can be generated. Three types of experiments were conducted: (i) VIV of a single flexible pipe of a circular cross section as the reference case, (ii) VIV of a single flexible pipe of a cactus-shaped cross section, and (iii) VIV of two tandem-arranged flexible pipes of the same cross-sectional shape (either circular- or cactus-shape). Figure 9 shows the test setup. Each pipe is connected to a steel

frame through cardan joints (universal joints) at both ends of the pipe. The columns of the steel frame are far away from the pipes, so their effects are assumed to be negligible. The frame is stiff enough and its natural frequency is much larger than the oscillating frequencies of the flexible pipes.

Figure 8. Water tunnel facility located in the Ocean Engineering Laboratory of China University of Petroleum (East China).

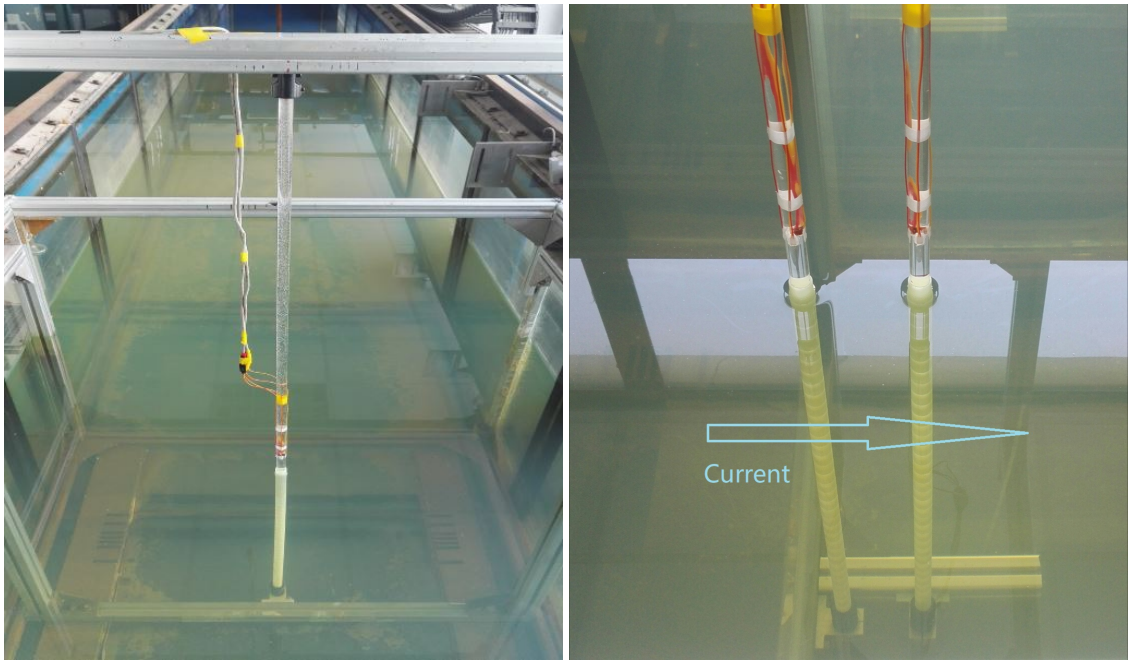

(**a**) Single pipe (**b**) tandem-arranged pipes

Figure 9. Experimental setup of (**a**) a single flexible pipe, and (**b**) a pair of tandem-arranged pipes of the same cross-sectional shape.

Sensor arrangement is shown in Figure 10. The length of pipes, measured between rotational axes of cardan joints attached at the pipe's ends, is 1.5 m. The pipe is partially submerged in the water. The water depth (measured from the rotational axis of the lower cardan joint) is 0.7 m. The pipe is sealed at its bottom end and fully filled with water to its top end. For the reduced velocity range considered in this study, the flexible pipes, either isolated or tandem-arranged, were excited to oscillate at its first mode, which was

proved theoretically by comparing the pipe's natural frequency and the vortex-shedding frequency, as well as by the observation. Thus, four strain sensors are attached on the outer circumference of the pipe at its mid-span location to measure the dynamic responses of the pipe. Sensors IL No. 1 and No. 2 are used to measure the strains of pipe in the in-line (IL) direction, which is the direction along the current flow; and sensors CF No. 1 and No. 2 are used to measure the strains of pipe in the cross-flow (CF) direction, which is the direction transverse to the direction of the current flows. In order to remove the tension strains, the total strains measured by the sensors are processed using the following equations to calculate the bending strains in the CF- and IL-direction, i.e., ε_{CF} and ε_{IL} can be expressed as:

$$\varepsilon_{CF} = \frac{\varepsilon_{CF2} - \varepsilon_{CF1}}{2}; \varepsilon_{IL} = \frac{\varepsilon_{IL2} - \varepsilon_{IL1}}{2} \quad (1)$$

where ε_{CF1} and ε_{CF2} are the strains measured by the sensors CF no. 1 and no. 2, respectively; and ε_{IL1} and ε_{IL2} are the strains measured by the sensors IL no. 1 and no. 2, respectively.

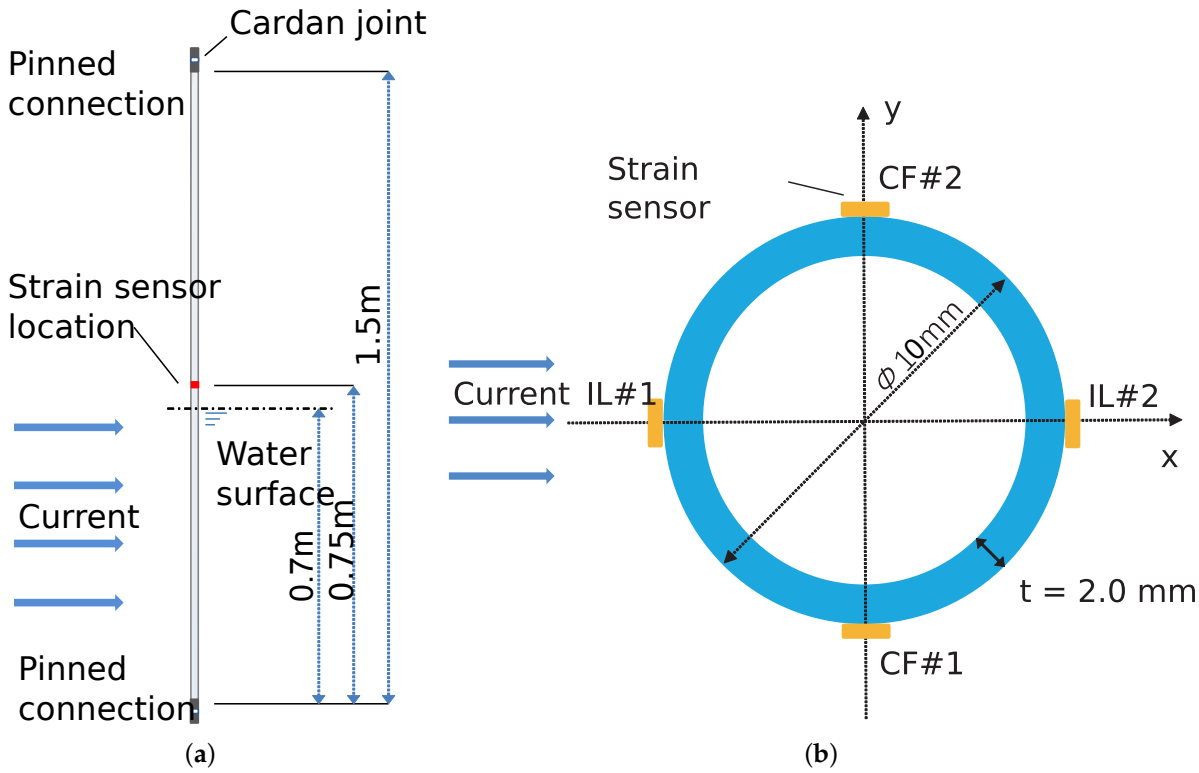

Figure 10. Strain sensor arrangement: (**a**) a side view of a pipe; and (**b**) four strain sensors attached on the circumference of the pipe at its mid-span location.

The flexible pipe is made of polycarbonate (PC) and of an outer diameter of 10 mm. As shown in Figure 11, five types of 3D-printed sleeves were used to alter the cross-sectional shape of the pipe. The flexible pipe with cactus-shaped sleeves attached on was used to study VIV responses of a cactus-shaped cylinder. Attached sleeves added mass on the flexible pipe. In order to make a suitable comparison, the same flexible pipe with circular sleeves attached on was used to resemble a circular cylinder, which was used as the reference case similar to the reference case of the numerical simulations. The sleeves were cut into short pieces each of a length of 17 mm and evenly distributed on the pipe with a narrow gap of 2 mm between the neighboring sleeves. The cactus-shaped sleeves installed onto the pipe have a staggered pattern, i.e., ridges are aligned with grooves of the neighboring sleeves. This staggered arrangement was used to weaken the spatial synchronization of vortex formation and shedding. The purpose of using short section of

sleeves and leaving gaps among them is to reduce the effects of sleeves on the bending stiffness of the pipe and to avoid collisions of neighboring sleeves when pipe oscillates. In addition, the sleeves were made of the same material and were designed to have the same cross-sectional area, thus, the mass of the five types of sleeves (including cactus-shaped sleeves and circular sleeves) are identical. As a result, dynamic characteristics, including the mass, bending stiffness, and natural frequencies of the flexible pipe attached with different cactus-shaped sleeves are almost identical to those of the pipe with circular sleeves attached on; which were verified by the free vibration tests discussed at below. Thus, VIV responses of a cactus-shaped cylinder can be directly compared with those of a circular cylinder through water tunnel experiments. As show in Figure 11, the circular sleeves, having an outer diameter of $D = 12$ mm and an inner diameter of $d = 10.2$ mm, were installed onto the flexible pipe to resemble a flexible circular cylinder of an diameter of 12 mm, which is the reference case and is labeled as $R0$. For cactus-shaped cylinders tested in this study, the height of ridges, h, is 4% of the cross-sectional diameter of the circular cylinder, i.e., $h = 12 \times 0.04 = 0.48$ mm. The minimum diameter, D_{min}, measured between the opposite ridge's dips, equals to 12 mm, which is the same as the outer diameter of the circular cylinder; and the maximum diameter, measured between the opposite ridge's tips, equals to $D_{max} = D + 2h = 12.96$ mm. The number of ridges of the four cactus-shaped sleeves are 8, 12, 16, and 20, so the cactus-shaped pipes are labeled as $R8$-0.04, $R12$-0.04, $R16$-0.04, and $R20$-0.04, respectively.

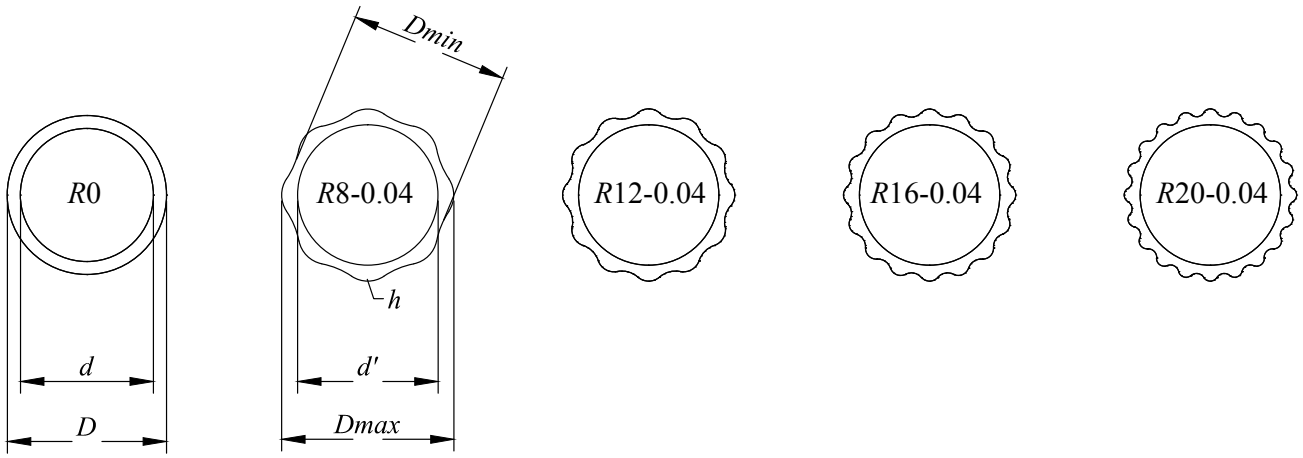

Figure 11. Sleeves of different cross-sectional shapes: circular $R0$ and cactus-like $R8$-0.04, $R12$-0.04, $R16$-0.04, $R20$-0.04.

5. Fundamental Natural Frequency and Free Vibration Test

For a uniform beam with pinned-pinned boundaries at both ends, the fundamental natural frequency, f_0, can be calculated based on the Euler-Bernoulli beam theory using Equation (2) at below:

$$f_0 = \frac{\pi}{2L^2}\sqrt{\frac{EI}{m}} \tag{2}$$

where L is the length of the beam, EI and m are the bending stiffness and linear mass density (mass per unit length of the beam), respectively.

In the present study the tested pipe was partially submerged in water, and the submerged section was covered by short sleeves either of a circular- or cactus-shaped cross section. The bending stiffness of the pipe, EI, is constant; however, the linear mass density, m, takes different values for the pipe section below and above the water level, which can be expressed as:

$$m(x) = \begin{cases} m_p + m_w + m_s + C_a m_d & \text{for } 0 \leqslant x \leqslant 0.7\,\text{m} \\ m_p + m_w & \text{for } 0.7\,\text{m} < x \leqslant 1.5\,\text{m} \end{cases} \tag{3}$$

where x is the coordinate along the length of pipe; m_p, m_w and m_s are the mass of inner pipe per unit length, mass of water inside the pipe per unit length, and mass of sleeve per unit length, respectively; m_d is the mass of displaced water per unit length and the added mass coefficient is assumed to take the value of $C_a = 1$ in this study. Note that, only the submerged section of pipe ($0 \leqslant x \leqslant 0.7$ m) is covered by sleeves, so the mass of sleeves and added mass of displaced water only be considered for the this section. Basic physical and hydrodynamic properties of the flexible pipe are summarized in Table 3.

Table 3. Basic physical and hydrodynamic properties of the flexible pipe.

Length, L	1500 mm
Outer diameter of inner pipe, d_0	10 mm
Wall thickness of inner pipe, t	2 mm
Mass of inner pipe per unit length, m_p	0.059 g/mm
Mass of water in pipe per unit length, m_w	0.028 g/mm
Mass of sleeves per unit length (submerged section), m_s	0.032 g/mm
Mass of displaced water per unit length (submerged section), m_d	0.108 g/mm
Equivalent linear mass density of pipe, m_{equ}	0.148 g/mm
Mass ratio	1.1
Modulus of elasticity, E	3.2 GPa

Lenci et al. [24] proposed a method to estimate the natural frequencies of a non-uniform beam. Based on their method, Equation (2) still can be used with the linear mass density, m, replaced by an equivalent linear mass density, m_{equ}, and expressed as:

$$m_{equ} = \frac{\int_0^L m(x)v^2(x)dx}{\int_0^L v^2(x)dx} \tag{4}$$

where L=1.5 m is the length of pipe. $v(x)$ is the mode shape function which may be approximated as a sine function, i.e., $v(x)$=$sin(\pi x/L)$, for this simple pinned-pinned flexible pipe. The equivalent linear mass density of the partially submerged flexible pipe can be calculated as $m_{equ} = 0.148$ g/mm and, further, the fundamental natural frequency is calculated as f_0 = 2.12 Hz.

Free vibration tests of a single pipe partially submerged in still water were carried out, and the time series of strains were measured at the mid-span location of the pipe. Natural frequencies of the pipes, partially covered by the five types of sleeves, were estimated from the power spectral of the free vibration strain time series. The values of the natural frequencies calculated from the measurements are all around 1.95 Hz for the pipes installed with sleeves, either of a circular or cactus-shaped cross section. The natural frequencies calculated from the measurements are consistent with the value calculated theoretically.

Note that the free vibration test was conducted and the natural frequency was calculated several times through the entire experimental program. Natural frequencies of all pipes remained unchanged before and after each VIV test run, which ensured that the experimental setup, including the boundary conditions, were consistent throughout the experimental program. Because only the submerged section of pipe was covered by sleeves, the mass ratio of the submerged section was calculated, which is expressed as the ratio of the linear mass density of pipe including the internal water and sleeves, $m_p + m_w + m_s$, divided by the mass of displaced water, m_d. The mass ratio is about 1.10, which is in the range of that for a real marine riser.

6. Water Tunnel Tests on a Single Flexible Pipe

VIV experiments on a single pipe installed with the five different sleeves, i.e., $R0$, $R8$-0.04, $R12$-0.04, $R16$-0.04, and $R20$-0.04, were conducted in the water tunnel at various reduced velocities $V_r = U/(f_0 D)$, where f_0 is the natural frequency of the pipe partially submerged in water. For our water tunnel facility, the maximum current speed is about 0.4 m/s, thus, several current speeds corresponding to a range of reduced velocities from

2 to 14 were tested. Bending strains at the mid-span location of the pipe in the IL- and CF-directions were measured with a sampling frequency of 200 Hz, and a stationary section, usually contains over 30 cycles of oscillations, were used to perform statistical analysis of the strains. Test results obtained from the four cactus-shaped sleeves, *R*8-0.04, *R*12-0.04, *R*16-0.04, and *R*20-0.04, share great similarities, and only the results of the cactus-shaped cylinder *R*8-0.04 was illustrated for the purpose of demonstrations. Figure 12 shows that the RMS values of micro-strains in the CF- and IL-direction, $\varepsilon_{\text{CF, RMS}}$ and $\varepsilon_{\text{IL, RMS}}$, of the cactus-shaped cylinder are much smaller than those of the circular pipe. One thing needs to be mentioned here is that IL VIV is often observed on many studies at the reduced velocity (Vr) from 1 to 4 [12,14,15,25]. However, the purpose of the present study is to compare the largest VIV response (CF VIV) of a cactus-shaped cylinder with that of a circular cylinder. With measures only at two reduced velocities (Vr is about 2 and 3.5), it is hardly to observe IL VIV on Figure 12.

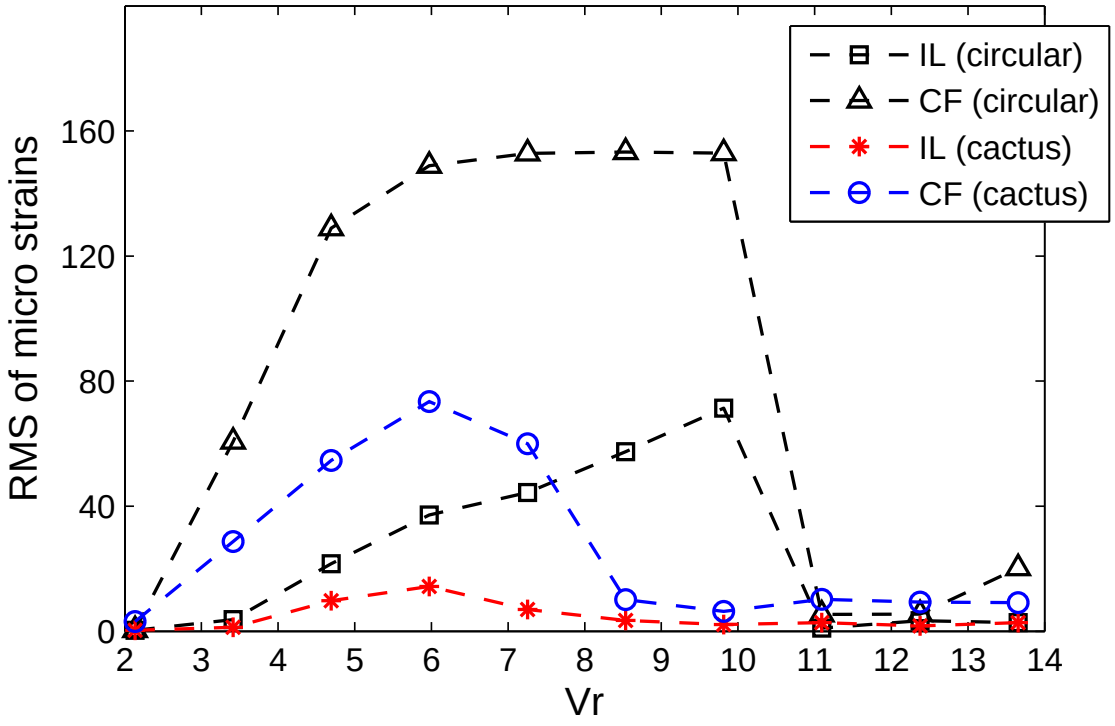

Figure 12. VIV responses of the cactus-shaped cylinder *R*8-0.04 and the circular cylinder *R*0 at various reduced velocities.

Figure 13 presents a 15-second time series of the micro-strains measured on the cylinders at the reduced velocity $V_r = 6$, where the IL and CF micro-strains of the pipe equipped with the cactus-shaped sleeve, *R*8-0.04, are plotted against with those of the pipe equipped with the circular sleeve, *R*0. The solid blue lines represent strains measured on the pipe equipped with the circular sleeves, and the red dotted lines represent strains measured on the pipe equipped with the cactus-shaped sleeves. The RMS values of the CF micro-strains, $\varepsilon_{\text{CF, RMS}}$, and the IL micro-strains, $\varepsilon_{\text{IL, RMS}}$, and the mean value of the IL micro-strains, $\varepsilon_{\text{IL, mean}}$, were calculated. The dominant frequencies of the CF and IL micro-strains, i.e., f_{CF} and f_{IL}, were estimated from the spectral analysis of the strain time series. Results were summarized in Table 4.

At the reduced velocity of 6, $\varepsilon_{\text{CF, RMS}}$, $\varepsilon_{\text{IL, RMS}}$, and $\varepsilon_{\text{IL, mean}}$ measured on the circular pipe are 154.0, 38.7, and 185.2, respectively; while, the values of the same parameters measured on the cactus-shaped cylinder, *R*8-0.04, are 71.6, 18.1, and 166.9, respectively, which are 53.5%, 53.2%, and 9.9% less than those of the circular cylinder. The dominant frequencies of the CF and IL micro-strains, f_{CF} and f_{IL}, of the cactus-shaped cylinder are slightly larger than those of the circular cylinder. The results show that the cactus-

shaped cylinder studied can reduce the VIV responses without increasing the drag. The observations are consistent with the numerical simulations.

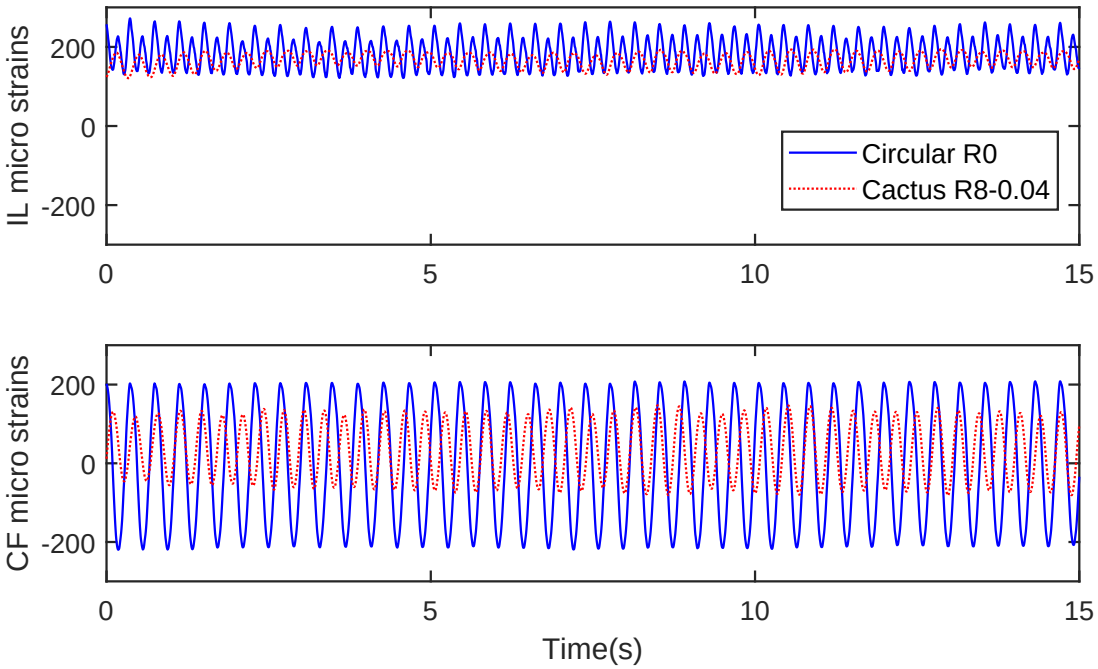

Figure 13. Micro-strains measured in the CF- and IL-directions at the mid-span location of a single flexible pipe installed with a circular sleeve, *R*0, and compared with those of a cactus-shaped sleeve, *R*8-0.04.

Table 4. VIV responses of a single flexible pipe with a different cross-sectional shape: circular *R*0 vs. cactus-shaped *R*8-0.04.

Para.	ε_{CF} **(RMS)**	ε_{IL} **(RMS)**	ε_{IL} **(Mean)**	f_{CF}	f_{IL}
Circular *R*0 (Ref.)	154.0	38.7	185.2	2.7	5.5
Cactus-shaped *R*8-0.04	71.6	18.1	166.9	2.9	5.8
difference (%)	−53.5	−53.2	−9.9	+7.4	+5.5

7. Water Tunnel Tests on Two Tandem-Arranged Flexible Pipes

In the previous section VIV tests on a single flexible pipe show that the cactus-like body shape reduce the dynamic VIV responses at various reduced velocities. In deepwater applications several marine risers are often placed in a group. Hydrodynamic responses of a riser in a group are different and much more complicated than those of an isolated riser. A riser sitting at the downstream position can be excited by the unsteady vortex-structural interaction between the riser and the vortices coming from the upstream riser, which differs from VIV and is termed wake-induced-vibration (WIV) [9]. Two tandem-arranged flexible pipes of the same cross-sectional shape, either of a circular shape, *R*0 or a cactus-shape, *R*8-0.04, were tested in the water tunnel to evaluate the effectiveness of the cactus-like body shape in the suppression of VIV or WIV considering the wake effects. Reduced velocities between 2 to 14 were considered. Center-to-center distances of the two pipes were set as 4*D*, 5*D*, 6*D*, 7*D* and 8*D*, where *D* is the outer diameter of the circular cylinder, *R*0. A spacing smaller than 4*D* was not considered in the present work, because when a riser experiencing VIV, its oscillation amplitude is possible to reach to a value larger than its outer diameter [26], and the minimum center-to-center distance between two risers should be larger than three times of the riser's diameter in order to avoid clashing with each other.

The dynamic responses for the two flexible pipes of different streamwise spacings were presented in Figure 14. The RMS values of the micro-strains measured on the upstream

and downstream pipes were presented. The black square and black triangle symbols represented the IL and CF responses of the circular pipes; and the red asterisk and blue circle symbols represented the IL and CF responses of the cactus-shaped pipes. Several conclusions can be observed:

(a) The upstream flexible pipe exhibits typical VIV behaviors. For example, the dynamic responses of the circular pipe increase with the reduced velocity from 2 to 5, then reach to a plateau at the reduced velocity from 5 to 10, and dramatically decrease as the reduced velocity larger than 10. The RMS values of both IL and CF micro-strains of the cactus-shaped pipe are greatly less than those of the circular pipe for the streamwise spacing from 4D to 8D. The reduced velocity lock-in range of the cactus-shaped pipe is also narrower than that of the circular pipe. These observations are consistent with those of the single flexible pipe shown in Figure 12 and prove that cactus-like body shape mitigate the VIV responses of the upstream pipe;

(b) Unlike the upstream flexible pipe, the downstream pipe is characterized by a galloping-like behavior, i.e., the dynamic responses remain relatively large even when the reduced velocity is greater than 10. Even through the dynamic responses of the downstream cactus-shaped pipe are less than those of the single circular pipe (compared with Figure 12), the RMS values of both IL and CF micro-strains of the downstream cactus-shaped pipe are generally comparable to those of the downstream circular pipe, which means that the cactus-like body shape modeled in this study does not effectively suppress WIV of the downstream pipe. Other researchers also observe that the mitigation efficiency of helical strakes on the WIV of the downstream pipe is significantly reduced [11]. The reason is that although the cactus-like body shape reduces strength of vortices shed from itself; while, the downstream pipe is mainly excited by the unsteady vortex-structural interaction between itself and the vortices coming from the upstream pipe, thus, the downstream pipe still experiences large oscillations.

(c) For the streamwise spacing from 4D to 8D tested in this study, the response of downstream pipe is dominated by WIV. This observation is consistent with a previous work of Assi et al. [9] which shows that vortex-shedding from the upstream pipe influences the downstream pipe for a wide range of the streamwise spacing, which may be up to 20 times of the pipe's diameter.

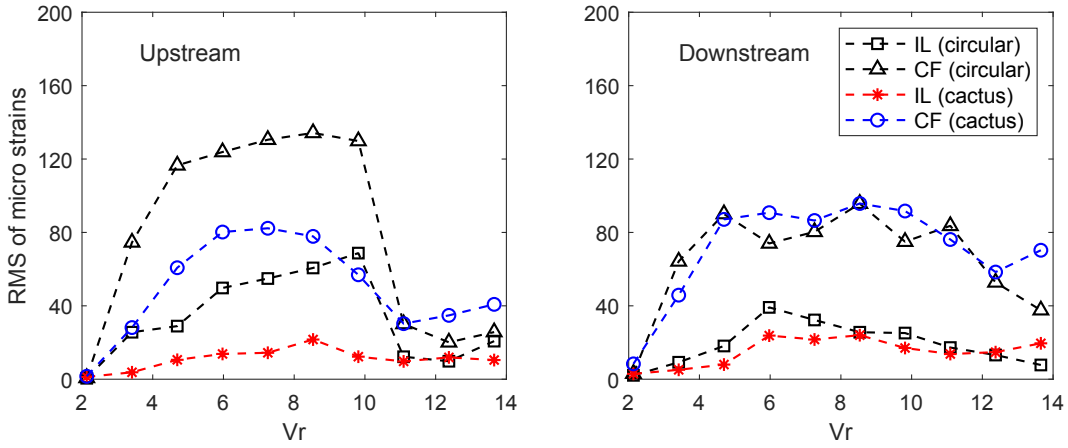

(**a**) Streamwise Spacing of 4*D*

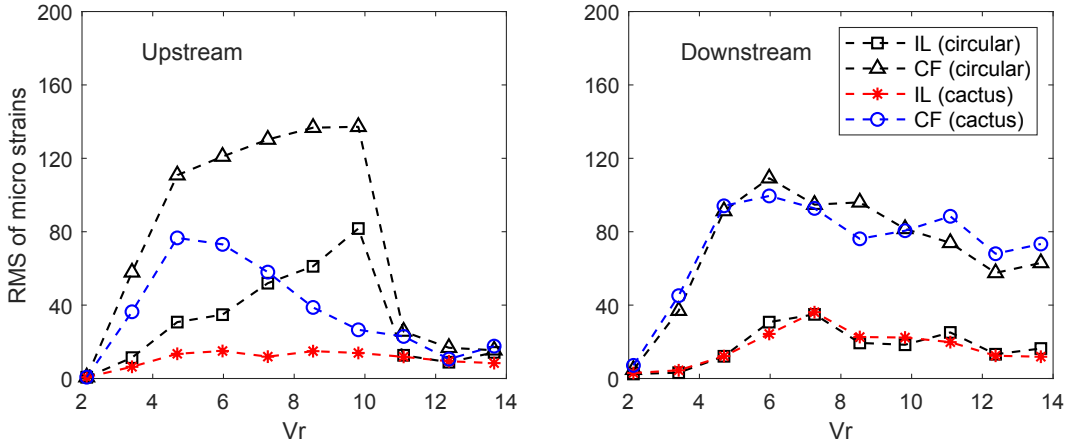

(**b**) Streamwise Spacing of 5*D*

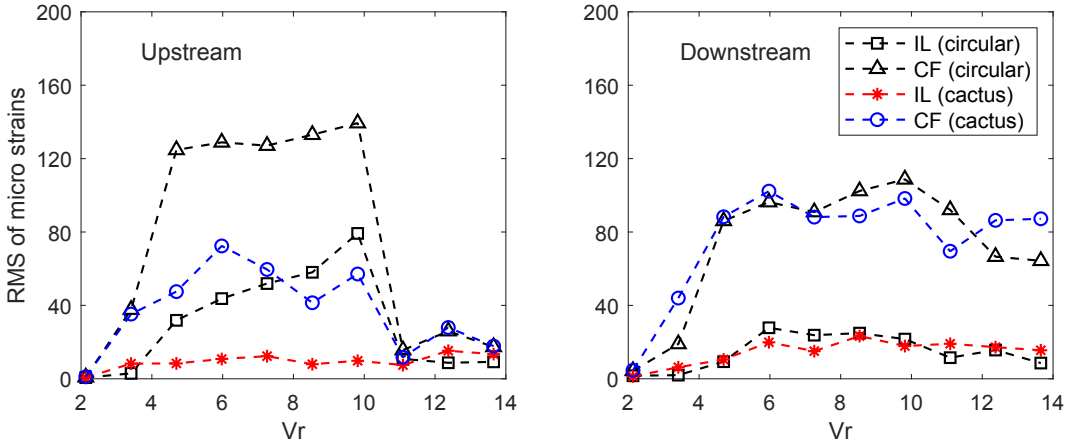

(**c**) Streamwise Spacing of 6*D*

Figure 14. *Cont.*

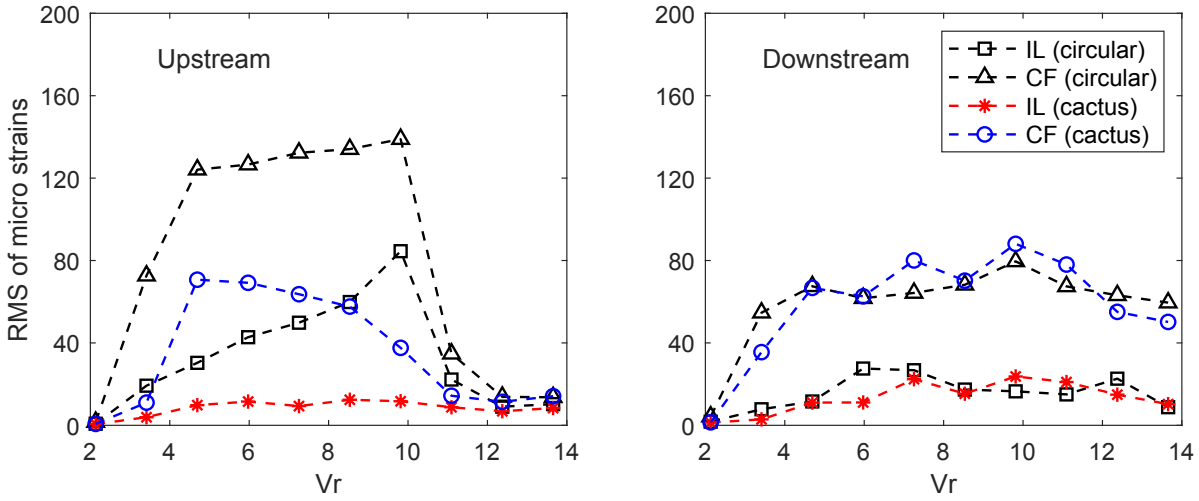

(**d**) Streamwise Spacing of 7*D*

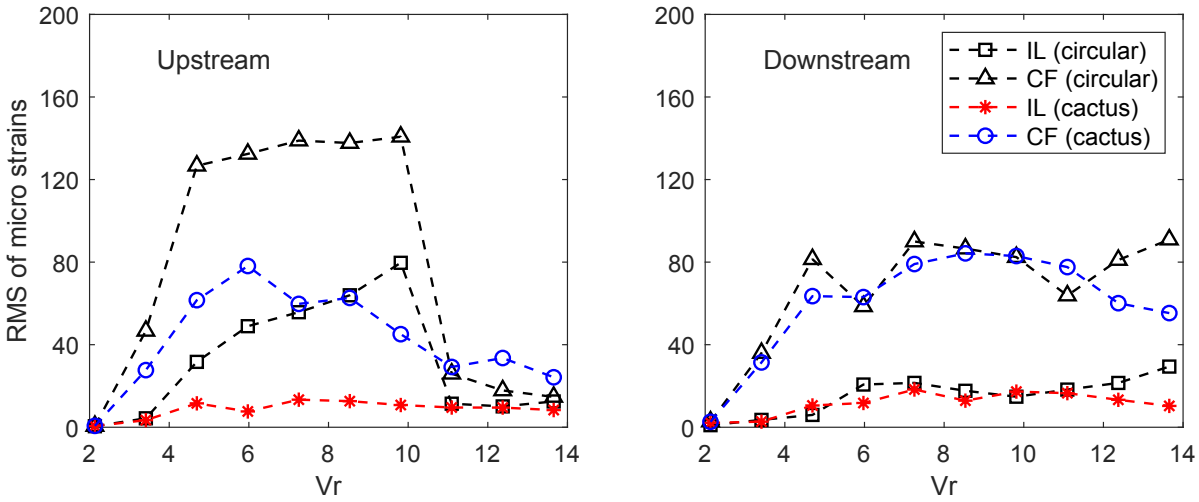

(**e**) Streamwise Spacing of 8*D*

Figure 14. Comparison of dynamic responses measured on the two cactus-shaped and circular shaped flexible pipes: (**a**) Streamwise spacing of 4*D*, (**b**) Streamwise spacing of 5*D*, (**c**) Streamwise spacing of 6*D*, (**d**) Streamwise spacing of 7*D*, and (**e**) Streamwise spacing of 8*D*.

8. Conclusions

In this study a uniform current flows past a single stationary cylinder was simulated in a two-dimensional flow field at a subcritical Reynolds number of $Re = 3900$ using the commercial software ANSYS FLUENT. Two type of cylinders were considered: a circular cylinder of a diameter of D used as the reference case and a cactus-shaped cylinder. By varying the number of ridges $n = 8, 12, 16, 20, 24$, and the height of ridges, $h = 0.02D, 0.04D, 0.06D, 0.08D$, systematically, twenty different cactus-shaped cylinders were considered. Results of simulations show that cactus-shaped cylinders may have smaller lift coefficients and Strouhal numbers than those of the circular cylinder, while the drag coefficients does not increase too much, which indicates that a cactus-like body shape may have reduced VIV response of a cylinder. Water tunnel experiments were conducted on a single flexible pipe exposed to a uniform current of reduced velocities varying from 2 to 14. The cross-sectional shape of the pipe was altered by installing different sleeves on it; one circular cylinder and four different cactus-shaped cylinders were tested. Experimental results show that

the cactus-like body shape can mitigate the VIV responses of the flexible pipe at no cost of significantly increased drag, which was consistent with the numerical simulations on a stationary cylinder. Additionally, water tunnel experiments on a set of two tandem-arranged flexible pipes with different streamwise spacings were conducted to investigate the VIV and WIV suppression efficiency of the cactus-like body shape. Results show that the cactus-like body shape studied in the present work reduces the dynamic responses of the upstream cylinder; while, similar to the helical strakes, the suppression efficiency is significantly reduced for the downstream cylinder.

The present work shows that the cactus-like body shape can mitigate VIV responses of cylinders; one advantage over helical strakes is that the drag force on the cylinder is not significantly increased. Two points need to be mentioned. First, the cactus-like body shape considered in this study was not optimized for VIV or WIV suppression; if well designed, the suppression efficiency is expected to be further improved. Second, VIV experiments using flexible cylinders were conducted in a subcritical Reynolds number flow field, the VIV mitigation efficiency of the cactus-like body shape should be further studied before being applied on marine risers exposed to real ocean current with a Reynolds number in the range of 10^5 to 10^6.

Author Contributions: J.W. was responsible for all the computations, simulations, and original draft preparation; F.C. was responsible for the experiments; C.S. was responsible for overall direction and review of the work and manuscript drafts; J.Y. assisted with problem definition and oversight. All authors have read and agreed to the published version of the manuscript.

Funding: Financial supports by National Key R&D Program of China "Research, development and project demonstration of a multipurpose flexible pipe for ultra-deepwaters (Grant No. 2016YFC0303800)."

Institutional Review Board Statement: Not applicable.

Informed Consent Statement: Not applicable.

Data Availability Statement: Not applicable.

Conflicts of Interest: The authors declare no conflict of interest. The founding sponsors had no role in the design of the study; in the collection, analyses, or interpretation of data; in the writing of the manuscript, or in the decision to publish the results.

Abbreviations

The following abbreviations are used in this manuscript:

CF	Cross-flow
CFD	Computational fluid dynamics
IL	Inline
RMS	Root-mean-square
VIV	Vortex-induced vibration
WIV	Wake-induced vibration

References

1. Talley, S.; Mungal, G. Flow around cactus-shaped cylinders. *Cent. Turbul. Res. Annu. Res. Briefs* **2002**, *2002*, 363–376.
2. Abboud, J.E.; Karaki, W.S.; Oweis, G.F. Particle image velocimetry measurements in the wake of a cactus-shaped cylinder. *J. Fluids Eng.* **2011**, *133*, 094502. [CrossRef]
3. Levy, B.; Liu, Y. The effects of cactus inspired spines on the aerodynamics of a cylinder. *J. Fluids Struct.* **2013**, *39*, 335–346. [CrossRef]
4. Babu, P.; Mahesh, K. Aerodynamic loads on cactus-shaped cylinders at low Reynolds numbers. *Phys. Fluids* **2008**, *20*, 035112. [CrossRef]
5. Marcollo, H.; Potts, A.E.; Johnstone, D.R.; Pezet, P.; Kurts, P. Drag Reduction and VIV Suppression Behaviour of LGS Technology Integral to Drilling Riser Buoyancy Units. In Proceedings of the 35th International Conference on Ocean, Offshore and Arctic Engineering (OMAE2016), Busan, Korea, 19–24 June 2016.
6. Tang, G.; Chen, C.; Zhao, M.; Lu, L. Numerical simulation of flow past twin near-wall circular cylinders in tandem arrangement at low Reynolds number. *Water Sci. Eng.* **2015**, *8*, 315–325. [CrossRef]

7. Sharman, B.; Lien, F.S.; Davidson, L.; Norberg, C. Numerical predictions of low Reynolds number flows over two tandem circular cylinders. *Int. J. Numer. Methods Fluids* **2005**, *47*, 423–447. [CrossRef]
8. Meneghini, J.R.; Saltara, F.; Siqueira, C.; Ferrari, J.A. Numerical simulation of flow interference between two circular cylinders in tandem and side-by-side arrangements. *J. Fluids Struct.* **2001**, *15*, 327–350. [CrossRef]
9. Assi, G.R.S.; Bearman, P.W.; Carmo, B.S.; Meneghini, J.R.; Sherwin, S.J.; Willden, R.H.J. The role of wake stiffness on the wake-induced vibration of the downstream cylinder of a tandem pair. *J. Fluid Mech.* **2013**, *718*, 210–245. [CrossRef]
10. Assi, G.R.S. Wake-induced vibration of tandem and staggered cylinders with two degrees of freedom. *J. Fluids Struct.* **2014**, *50*, 340–357. [CrossRef]
11. Huang, S.; Sworn, A. Hydrodynamic coefficients of two fixed circular cylinders fitted with helical strakes at various staggered and tandem arrangements. *Appl. Ocean. Res.* **2013**, *43*, 21–26. [CrossRef]
12. Sumer, B.; Fredsøe, J. *Hydrodynamics around Cylindrical Structures (Revised Edition), Advanced Series on Ocean Engineering, Volume 26*; World Scientific Publishing: Singapore, 2006.
13. Sarpkaya, T. Hydrodynamic Damping, Flow-Induced Oscillations, and Biharmonic Response. *ASME. J. Offshore Mech. Arct. Eng.* **1995**, *117*, 232–238. [CrossRef]
14. Jauvtis, N.; Williamson, C. The effect of two degrees of freedom on vortex-induced vibration at low mass and damping. *J. Fluid Mech.* **2004**, *509*, 23–62. [CrossRef]
15. Blevins, R.; Coughran, C. Experimental Investigation of Vortex-Induced Vibration in One and Two Dimensions with Variable Mass, Damping, and Reynolds Number. *J. Fluids Eng.* **2009**, *131*, 101202. [CrossRef]
16. Franzini, G.; Pesce, C.; Gonçalves, R.; Fujarra, A.; Pereira, A. Concomitant vortex-induced vibration experiments: A cantilevered flexible cylinder and a rigid cylinder mounted on a leaf-spring apparatus. *J Braz. Soc. Mech. Sci. Eng.* **2014**, *36*, 547–558. [CrossRef]
17. Swithenbank, S.; Vandiver, J.; Larsen, C.; Lie, H. Reynolds number dependence of flexible cylinder VIV response data. In Proceedings of the ASME 2008 27th International Conference on Offshore Mechanics and Arctic Engineering, Estoril, Portugal, 15–20 June 2008; pp. 503–511.
18. Kang, Z.; Zhang, C.; Chang, R.; Ma, G. A numerical investigation of the effects of Reynolds number on vortex-induced vibration of the cylinders with different mass ratios and frequency ratios. *Int. J. Nav. Archit. Ocean. Eng.* **2019**, *11*, 835–850. [CrossRef]
19. Belloli, M.; Giappino, S.; Morganti, S.; Muggiasca, S.; Zasso, A. Vortex induced vibrations at high Reynolds numbers on circular cylinders. *Ocean. Eng.* **2015**, *94*, 140–154. [CrossRef]
20. Ren, T.; Zhang, M.; Fu, S.; Song, L. Hydrodynamics of A Flexible Riser Undergoing the Vortex-Induced Vibration at High Reynolds Number. *China Ocean. Eng.* **2018**, *32*, 570–581. [CrossRef]
21. Fröhlich, J.; Rodi, W.; Kessler, P.; Parpais, S.; Bertoglio, J.P.; Laurence, D. Large eddy simulation of flow around circular cylinders on structured and unstructured grids. *Notes Numer. Fluid Mech.* **1998**, *66*, 319–338.
22. Pereira, F.S.; Vaz, G.; Eça, L.; Girimaji, S.S. Simulation of the flow around a circular cylinder at Re= 3900 with Partially-Averaged Navier-Stokes equations. *Int. J. Heat Fluid Flow* **2018**, *69*, 234–246. [CrossRef]
23. Jhingran, V.G. Drag Amplification and Fatigue Damage in Vortex-Induced Vibrations. Ph.D. Thesis, Massachusetts Institute of Technology, Cambridge, MA, USA, 2008.
24. Lenci, S.; Clementi, F.; Mazzilli, C.E.N. Simple formulas for the natural frequencies of non-uniform cables and beams. *Int. J. Mech. Sci.* **2013**, *77*, 155–163. [CrossRef]
25. Srinil, N.; Zanganeh, H.; Day, A. Two-degree-of-freedom VIV of circular cylinder with variable natural frequency ratio: Experimental and numerical investigations. *Ocean. Eng.* **2013**, *73*, 179–194. [CrossRef]
26. Posdziech, O.; Grundmann, R. Numerical simulation of the flow around an infinitely long circular cylinder in the transition regime. *Theor. Comput. Fluid Dyn.* **2001**, *15*, 121–141.